

Doppler measurement of implosion velocity in fast Z-pinch x-ray sources

B. Jones,^{1,*} C. A. Jennings,¹ J. E. Bailey,¹ G. A. Rochau,¹ Y. Maron,² C. A. Coverdale,¹ E. P. Yu,¹ S. B. Hansen,¹ D. J. Ampleford,¹ P. W. Lake,¹ G. Dunham,¹ M. E. Cuneo,¹ C. Deeney,^{1,†} D. V. Fisher,^{2,‡} V. I. Fisher,² V. Bernshtam,² A. Starobinets,² and L. Weingarten²

¹Sandia National Laboratories, Albuquerque, New Mexico 87185, USA

²Faculty of Physics, Weizmann Institute of Science, Rehovot 76100, Israel

(Received 8 December 2010; revised manuscript received 13 May 2011; published 28 November 2011)

The observation of Doppler splitting in *K*-shell x-ray lines emitted from optically thin dopants is used to infer implosion velocities of up to 70 cm/ μ s in wire-array and gas-puff *Z* pinches at drive currents of 15–20 MA. These data can benchmark numerical implosion models, which produce reasonable agreement with the measured velocity in the emitting region. Doppler splitting is obscured in lines with strong opacity, but red-shifted absorption produced by the cooler halo of material backlit by the hot core assembling on axis can be used to diagnose velocity in the trailing mass.

DOI: [10.1103/PhysRevE.84.056408](https://doi.org/10.1103/PhysRevE.84.056408)

PACS number(s): 52.58.Lq, 52.59.Qy, 52.70.La

I. INTRODUCTION

Doppler shifts of emission lines provide a powerful tool for measurement of bulk motion in physical systems. This spectroscopic technique is used to detect seismic activity in the sun [1], waves in the solar corona [2], the wobble of stars perturbed by exoplanets [3,4], and binary black holes in galaxy merger remnants [5]. In the laboratory, the Doppler effect reveals rotation in tokamaks [6,7] and ion flows created during magnetic reconnection of plasmas [8].

Gas-puff *Z* pinches at $\lesssim 3$ MA have exhibited Doppler splitting in 40- to 4000-Å *L*-shell emission lines due to radial implosion velocity [9–12]. Here, we extend the spectroscopic technique to measure Doppler implosion velocities by using time- and space-resolved 3- to 9-Å *K*-shell x-ray lines on the 15- to 20-MA *Z* pulsed power facility [13,14]. The high velocities (up to 70 cm/ μ s) and compact source sizes (few-millimeter radius of the imploding shell) attained on *Z* require nanosecond time resolution and submillimeter spatial resolution of the crystal spectrometers employed in order to study the time evolution of Doppler velocity.

Measurement of velocity is important to inferring the plasma kinetic energy, which can be the primary storage reservoir of $\mathbf{j} \times \mathbf{B}$ work accumulated over ~ 100 ns during implosion and then provide plasma heating when thermalized at stagnation. While some studies have shown consistent energy balance between kinetic energy input and radiated output [15–19], others have proposed that additional physical processes may provide further plasma heating [20–23]. Doppler velocity measurements will help to test models and address this key physics issue for high-current pinches [24].

The *Z* machine is the highest-power laboratory soft x-ray source, producing up to 250 TW and 1.8 MJ of radiation [25].

Intense *K*-shell emission is seen from low- to mid-atomic-number materials (Al to Cu) on *Z* [26] as the imploding plasma stagnates and is heated on its central axis. Observation of Doppler effects in these *K*-shell lines thus provides unique information about the plasma motion at the onset of stagnation.

In this paper, we present observations of Doppler shifts in a gas puff fielded at *Z* and show the extension of the technique to wire-array *Z* pinches, demonstrating the general applicability of the technique to fast magnetic implosions. We further present an initial comparison of Doppler measurements to a three-dimensional magnetohydrodynamic (3D MHD) implosion simulation and discuss an approach for constraining the modeled plasma velocity and coupled kinetic energy. For the *K*-shell x-ray radiation, many of the emission lines have high opacity, and we have also demonstrated for the first time that Doppler-shifted absorption can reveal the velocity in mass trailing the implosion. In this scenario, opacity can complicate the line shape and obscure Doppler splitting. However, *Z* pinches at the start of the stagnation process generally produce a hot, dense column on axis that emits brightly and can act to backlight the trailing material, which is cooler and still imploding. We show that a Doppler shift is observable in the subsequent absorption feature produced by the cooler halo, and we present a method using collisional radiative modeling and radiation transport calculations to simulate the measured line shape in order to infer velocity, temperature, and density of the trailing mass.

The Doppler phenomenon studied involves an imploding *Z*-pinch shell viewed from the side as in Fig. 1(a). A spectrometer which spatially resolves in the *x* direction will see emission lines Doppler split into red and blue components at $x = 0$ due to the opposing motion of the near and far sides of the shell, while a view at large *x* perpendicular to the velocity vector will see no splitting. Consider a cylinder (typical length 1–2 cm) with constant emissivity ϵ over radii $r_1 - r_2$ [Fig. 1(b)] moving with constant velocity $v = 50$ cm/ μ s [Fig. 1(c)]. Assuming the spectral line of interest is optically thin, an instrument viewing along the *y* axis chordally integrates the emission, $\int \epsilon dy = \int \epsilon(x, y) \frac{dy}{d\lambda} d\lambda = \int P(x, \lambda) d\lambda$. The term $\frac{dy}{d\lambda}$ is evaluated along the path of each chord at a particular position *x*, and the projection of the moving shell onto the

*bmjones@sandia.gov

†Present address: US DOE, National Nuclear Security Administration, Washington, DC 20585, USA.

‡Present address: University of California, Davis, California 95616, USA.

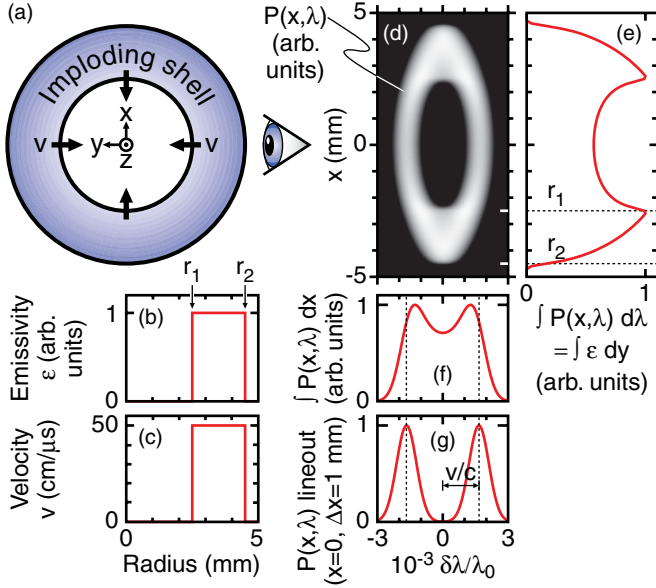


FIG. 1. (Color) Side-on observation of an imploding shell (a) with specified emissivity (b) and velocity (c) will produce an oval-shaped line profile (d) due to the Doppler effect when the spectrometer is spatially resolved in the x direction. The Abel forward transform (e) is recovered from this image when integrated over λ . A spectrometer with no spatial resolution integrates over x (f), while looking near $x = 0$ in the imaged spectrum (g) gives a clear measure of Doppler splitting.

imaging spectrometer is derived as

$$P(x, \lambda) = \epsilon \frac{c|x|}{v\lambda_0} \left(1 - \left(\frac{c\delta\lambda}{v\lambda_0} \right)^2 \right)^{-3/2}$$

$$\text{if } \frac{r_1^2 - x^2}{r_1^2} \leq \left(\frac{c\delta\lambda}{v\lambda_0} \right)^2 \leq \frac{r_2^2 - x^2}{r_2^2} \quad (1)$$

or zero if the condition is not met, where $\delta\lambda = \lambda - \lambda_0$ is the wavelength shift relative to the reference line wavelength λ_0 . At $x = 0$, Eq. (1) becomes two red-and-blue split δ functions at $\delta\lambda/\lambda_0 = \pm v/c$. Equation (1) is plotted in Fig. 1(d), convolved with the $\sim 200\text{-}\mu\text{m}$ spatial and $\lambda/\Delta\lambda \sim 900$ spectral resolution typical of the time-gated x-ray spectra to be presented. This image is a transform of the source's spatial structure, with the coordinate y mapped to λ and retaining information about velocity in the wavelength dimension due to the Doppler effect. Indeed, integrating the image over λ in Fig. 1(e) gives the standard limb-brightened image of the analytical Abel transform for an emitting shell. Oval-shaped line profiles dominated by Doppler splitting were previously observed from planetary nebula [27,28] in which a dying star casts off its outer layers to create a spherically expanding shell. The time and distance scales are quite different here, but the effect is geometric in nature and phenomenologically identical. The above discussion indicates that oval-shaped, Doppler split line profiles should be observable in fast, high-current Z pinches given the expected plasma sizes and velocities and the resolution of the instruments employed on Z.

Spatially resolving the oval line shape provides confidence that the feature is due to Doppler splitting and not due to adjacent emission lines or opacity at line center. The image in

Fig. 1(d) is integrated over x in Fig. 1(f), representing the line shape that would be measured by a spectrometer with no spatial resolution. Doppler splitting can still be seen, but it is obscured and the peaks shifted due to contributions from intensity at large x . In contrast, taking a lineout of the image at $x = 0$ [Fig. 1(g)] clearly shows the red and blue Doppler-shifted components at the expected spectral positions $\delta\lambda/\lambda_0 = \pm v/c$.

In Sec. II, we present Z data showing Doppler splitting of K-shell dopant lines in both gas-puff and wire-array Z pinches. A 3D MHD implosion model is also presented in the case of the wire-array configuration, and a path forward for quantitative comparison of velocity between model and experiment is discussed. Section III discusses how Doppler-shifted absorption may be used to infer velocity using high-opacity lines. Finally, Sec. IV reviews the Doppler spectroscopic techniques studied on Z and discusses potential future work.

II. DOPPLER SPLITTING OF LOW-OPACITY DOPANT LINES

A schematic of the instrument used to measure time- and space-resolved x-ray spectra on Z is shown in Fig. 2 [29,30]. An elliptically bent crystal provides dispersion, while a slit provides radial resolution for each $<1\text{-ns}$ -gated frame of a microchannel plate camera.

Example data are shown in Fig. 3 from an annular 80-mm-diameter deuterium gas puff of Coverdale *et al.* [31,32] doped with 0.5% (by number) Ar and 0.5% Freon R-12 (providing Cl). Oval shapes due to Doppler splitting are seen in all Ar and Cl lines during implosion. The temporal resolution of the detector is crucial to observing the oval-shaped lines in the earlier frames with adequately low motional blurring and to avoid washing out the Doppler splitting entirely by the intense emission at peak x-ray power (0 ns). Doppler splitting is seen when the plasma begins to emit K lines (approx. -10 ns) and disappears by 0 ns, presumably as kinetic energy is thermalized. Thus, this measurement technique can be used to infer plasma velocity during the final stage of implosion and the onset of stagnation.

Fitting two Gaussians plus a constant to lineouts through $x = 0$ [as in Fig. 1(g)] for the Ar He- β , Cl He- β , and Ar He- α lines gives velocities of 71, 66, and 68 cm/ μs respectively at -6 ns, and 58, 55, and 56 cm/ μs for the -3-ns frame. Uncertainties of $\pm 2\text{--}3$ cm/ μs combine least-squares fit errors

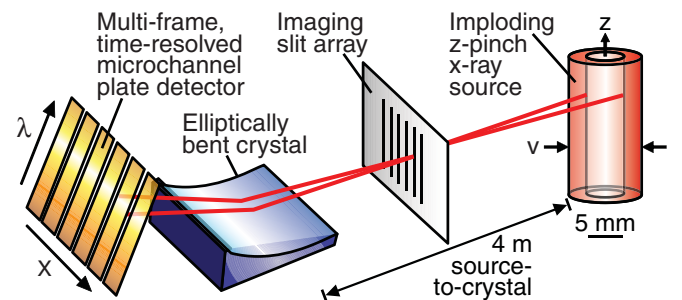


FIG. 2. (Color) A slit-imaging crystal spectrometer measures Doppler effects on the Z machine. A multiframe microchannel plate camera records time-gated soft x-ray spectra with one-dimensional (1D) spatial resolution.

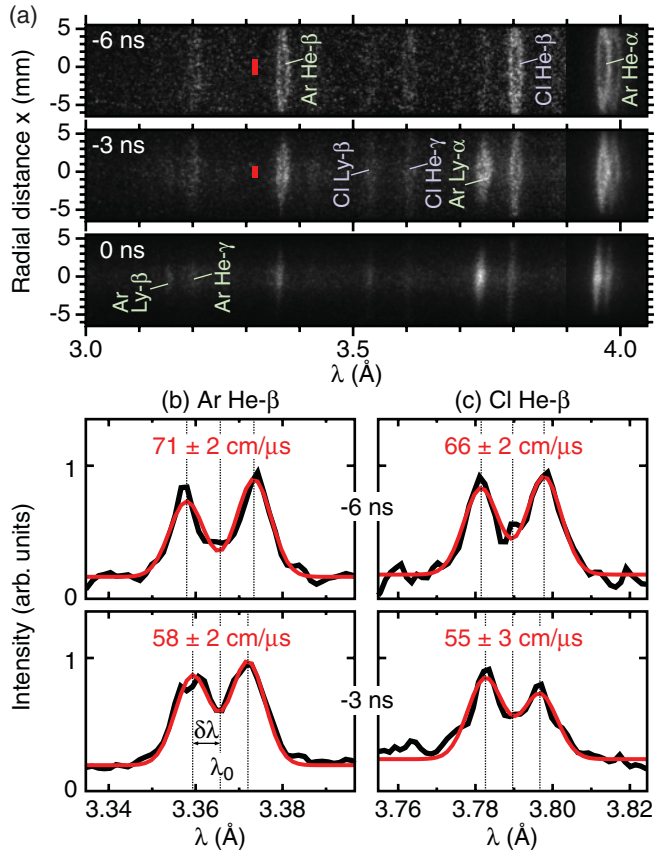


FIG. 3. (Color) (a) Time-gated, radially resolved, *K*-shell x-ray spectra are recorded on the Z machine. Ar and Cl dopants in a D₂ gas puff (Z1422) show Doppler splitting in the imploding shell, disappearing before peak radiated power (0 ns). The intensity of the Ar He- α line is reduced here for clarity. Lineouts over the spatial regions indicated with red bars are shown (black curves) for (b) Ar He- β and (c) Cl He- β along with fits (red) from which radial velocity is inferred. Deceleration of the emitting region is clearly seen from the -6-ns to the -3-ns frame.

in the peak positions with variation due to changing the data window used in the fit. We interpret these values as the emissivity-weighted average velocity and emphasize that the velocity is measured only in the region of the plasma that is emitting the particular line. Examples of these fits shown in Figs. 3(b) and 3(c) for Ar He- β and Cl He- β clearly show deceleration in the experimental data. These actual particle velocities are consistent with inferences from separate diagnostics and with prior numerical modeling [32], which also showed deceleration of the plasma at the onset of stagnation. In Ref. [32], the effective radius of current flow in the Z pinch was inferred through analysis of electrical circuit data [33], with peak velocity of ~ 70 cm/ μ s decreasing to ~ 40 cm/ μ s near stagnation. The ± 10 -cm/ μ s accuracy of this measurement was less constraining than the Doppler spectroscopy presented here, and the interpretation is more complicated as it is not a direct measure of particle velocity.

The observed trend of deceleration near the end of the implosion phase, when coupled with studies of the evolution of plasma temperature and density using line intensity ratios [34,35], could enhance understanding of plasma heating

during the gas-puff stagnation phase. In the work of Foord *et al.* [12], the authors studied Doppler splitting of oxygen lines in a CO₂ gas-puff Z pinch. Collisional radiative modeling of line ratios there allowed inference of plasma conditions and consequently provided a method for studying plasma ionization and momentum-transfer dynamics. Deceleration of particles near the axis was not seen in that work, but the plasma mass and pressure were low by comparison and the line emission was observed only >5 mm from the axis and at times earlier than -40 ns. The higher current (~ 20 MA versus 290 kA) and much shorter implosion time (~ 100 ns versus 600 ns) on Z may result in different implosion and stagnation dynamics.

Doppler splitting has also been observed from a 40-mm-diameter nested Al wire array with 1.5 mg/cm mass per unit length and a 5% Mg dopant. The oval-shaped Mg He- α line profile is seen to converge onto the pinch axis in Fig. 4(a), with splitting vanishing prior to peak x-ray power as was observed in the gas-puff data. In Fig. 4(b), a double-Gaussian fit (red) to an $x = 0$ lineout (black) through the -9-ns frame gives 52 cm/ μ s average velocity with less than $\pm 5\%$ error. This is consistent with the 53 ± 8 cm/ μ s velocity inferred by fitting a line (red) through the trajectory [black points in Fig. 4(c)] of the average radial position of Mg He- α emission taken from the spectrometer images where ovals are seen. This comparison demonstrates that precise instantaneous Doppler velocity can be measured in wire-array Z pinches through careful choice of emission line.

Doppler splitting reflects true particle velocity of the emitting material, while the presence of an ionization wave in some cases could produce a different apparent velocity in self-emission imaging [12]. The fact that these velocities are similar here suggests that in this case the emission tracks the

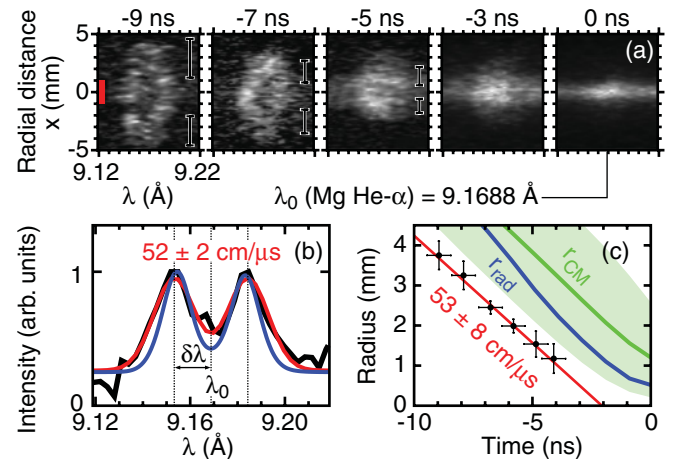


FIG. 4. (Color) (a) Doppler splitting of a Mg He- α dopant line in an Al wire array (Z1520) disappears as the emitting shell reaches the pinch axis (-3 and 0 ns from peak power). (b) A fit (red) to a lineout (black) over the spatial region indicated by the red bar in the -9-ns frame gives average velocity to less than $\pm 5\%$. The line shape from a 3D MHD model is compared (blue). (c) A linear fit (red) to the average radial position (black points) of the Mg He- α emission region [black bars in (a)] gives a consistent velocity with larger error. The center of radiation (blue) leads the center of mass (green) in the model; the shaded region is bounded by curves enclosing 10% and 90% of the mass.

mass flow. This may not be true for every plasma configuration, but it appears to be the case for both the wire-array and gas-puff Z implosions presented here. While fewer frames of data were available for the gas-puff experiment in Fig. 3, the $\sim 60\text{-cm}/\mu\text{s}$ velocity apparent from the change in radial position of the line emission from the -6- to the -3-ns frame is similarly consistent with the velocity inferred from Doppler splitting. Perhaps due to the faster implosion or differing plasma conditions on Z , thermal conduction apparently does not drive an ionization wave ahead of the magnetic piston as seen by Foord *et al.* [12]. This effect could preheat plasma on axis and modify the stagnation process, and so it merits further study.

This Al wire-array experiment was simulated with the 3D Eulerian resistive MHD code GORGON [19], with total emissivity ϵ_i in each $150\text{-}\mu\text{m}$ Cartesian cell estimated from tabulated non-local-thermodynamic-equilibrium (non-LTE) SCRAM/SC atomic code calculations [36,37]. Both the center-of-mass velocity and the simulated emissivity-weighted velocity reflected by a Doppler-splitting measurement were considered in the model. Comparison to the experimental data provides insight regarding the interpretation of the Doppler velocity. If Doppler velocity is indicative of the center-of-mass velocity, then we could directly infer the kinetic energy of the imploding plasma. As we will show, the two may not be equal and so care must be taken in the interpretation of the Doppler velocity measurements. These experimental data may still provide a valuable constraint on the numerical modeling, and we outline a procedure for comparing the two.

In Fig. 4(c), the radial center of mass is shown (green), defined as mass-weighted radius summed over the computational grid and divided by total mass. The similarly calculated center of emissivity (blue) leads the mass and stagnates on axis first, as seen in prior wire-array experiments [38]. As radiation is emitted predominantly by the leading edge of the imploding material according to the model, we might expect the inferred velocity from x-ray line Doppler splitting to be different than the center-of-mass velocity.

In order to compare the MHD model with measurements as directly as possible, we construct a synthetic Doppler-split line profile and infer a velocity from the degree of splitting as in the experiment. Simulated line shapes were constructed at various times as depicted in Fig. 5(a). Each cell was assigned a Doppler shift $\delta\lambda_i = \lambda_0 \vec{v}_i \cdot \hat{y}/c$ based on its velocity component along the viewing direction, all cell emissivities were binned versus λ , and the resulting line profile at $x = 0$ was convolved with the instrumental resolution. Despite the 3D instabilities seen in Fig. 5(a) (and present in Z wire-array experiments [14,39,40]), the plasma remains shell-like enough to exhibit well-defined Doppler splitting. One example (blue) in Fig. 4(b) shows splitting comparable to the experiment, indicating agreement in the emissivity-weighted velocity.

The simulated line broadening naturally includes velocity variations in the plasma; however, broadening due to thermal motion, opacity, or other effects may need to be included for quantitative agreement of the line shapes. Likewise, broadening of the red and blue peaks in the experimental data could be caused by velocity gradients in the emitting region of the plasma, finite ion temperature, or line opacity. Correlating the observed widths with plasma effects will also require careful accounting of the instrumental resolution at

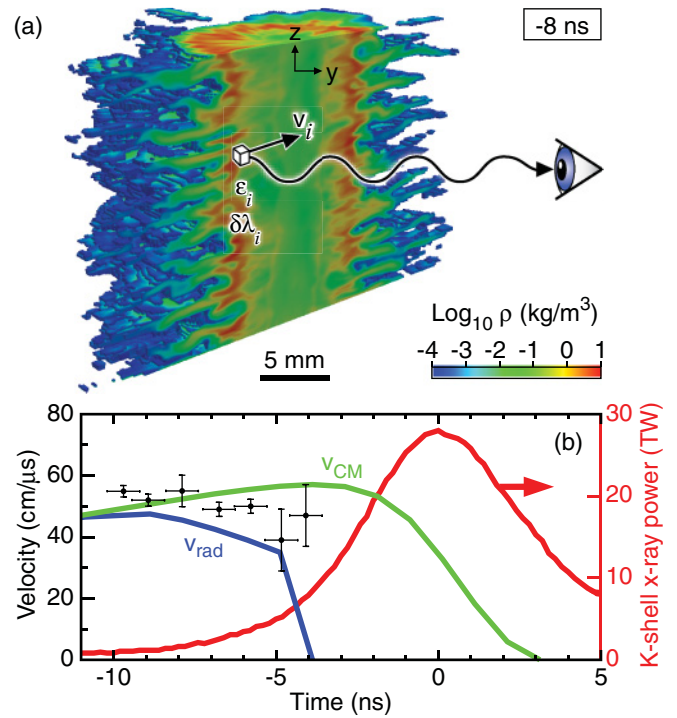


FIG. 5. (Color) (a) The density structure of a wire-array implosion in a 3D MHD model suggests that the implosion remains shell-like despite the presence of 3D magnetic Rayleigh-Taylor instabilities. Modeled Doppler splitting in Fig. 4(b) considers emissivity and viewing geometry for the 3D MHD grid cells. (b) Doppler velocity measurements (black points) are compared with modeled velocities. In the model, the velocity weighted by total radiation emissivity v_{rad} falls before the center of mass velocity v_{CM} as the emitting region reaches the axis and stagnates first. Here v_{rad} is $\sim 15\%$ below the measured average velocity of the Mg He- α emission region; the agreement might be improved by modeling the specific line emission. The measured K -shell x-ray pulse is shown for timing reference.

each wavelength where Doppler splitting is observed. Study of K -shell line widths on Z will be addressed further in future work. For the present discussion, we restrict ourselves to comparing the degree of Doppler splitting, indicating emissivity-weighted average velocity.

Finally, Fig. 5(b) shows the modeled center-of-mass velocity v_{CM} (green), along with the velocity of the radiation region v_{rad} (blue) calculated by fitting two Gaussians to the simulated line profiles, mimicking the experimental analysis. On average, v_{rad} is 15% lower than the measured velocity (black). More accurate comparison of Doppler velocities of the line-emitting region between experiment and code may require calculating the line emissivity specifically. To be pursued in future work, this will require generating a table of Mg He- α emissivity using SCRAM/SC and rerunning the GORGON model using this table to generate line shapes. It will also be interesting to use this particular line emissivity to assess the radial location of the emission region; at present, using the tabulated total emissivity, the emission region in the model lags the measured position of Mg He- α emission as shown in Fig. 4(c).

In the model [Fig. 5(b)], v_{rad} does not equal v_{CM} as the radiating region leads the mass and decelerates on axis first,

even as most of the mass continues to be accelerated by the $\mathbf{j} \times \mathbf{B}$ force. Due to the presence of gradients, Doppler velocity measurements do not necessarily allow a direct measurement of instantaneous kinetic energy of the entire plasma. They are weighted by emissivity of the particular line, which may emit from only a portion of the plasma. However, they still may provide leverage in constraining numerical models through direct comparison with simulated velocity as outlined above. Physics refinements bringing modeled velocities into closer agreement with experimental results will further test the kinetic energy coupling calculated in the code.

In the numerical model discussed here, the total radiated yield is explained by the ~ 600 -kJ/cm $\mathbf{j} \times \mathbf{B}$ -coupled energy. This total coupled energy exceeds the ~ 300 -kJ/cm peak instantaneous kinetic energy as has also been observed in previous two-dimensional (2D) [41] and 3D [42] MHD models. Recent GORGON simulations [19] suggest that additional anomalous heating mechanisms are not needed to explain the energy balance when the dynamics of distributed mass and current are appropriately accounted for. The 3D implosion instabilities produce a radially distributed shell, and a significant amount of $\mathbf{j} \times \mathbf{B}$ work is then performed on the trailing material during the stagnation of the plasma. In this manner, during stagnation kinetic energy is both created by $\mathbf{j} \times \mathbf{B}$ and simultaneously dissipated due to thermalization. It is thus unphysical to consider a final pinch kinetic energy at the end of a distinct implosion phase that subsequently provides all of the input to plasma heating. Rather, it is important to understand the time history of plasma kinetic energy during the stagnation process. Our strategy is to test these numerical models further by comparing instantaneous velocities extracted from simulated line shapes to the measured emissivity-weighted velocities. While not a direct measure of kinetic energy, constraining the model to match these Doppler velocities may add confidence that the model is producing the correct evolution of coupled kinetic energy. Using other dopant lines excited at lower temperature could probe trailing material in future experiments and potentially provide information on the velocity of a greater fraction of the imploding mass.

III. DOPPLER-SHIFTED ABSORPTION OF HIGH-OPACITY LINES

Some studies have indicated that trailing mass may shunt current and reduce kinetic energy coupling in Z pinches [38,43,44]. In contrast, other recent work has suggested that trailing mass can enhance $(\mathbf{j} \times \mathbf{B})$ -coupled energy by allowing $\mathbf{j} \times \mathbf{B}$ to continue doing work after stagnation has begun [19,45]. It is important to determine the structure and velocity of mass trailing the main implosion front in order to understand better the role that it plays in Z -pinch energy deposition, and the spectral analysis in this section provides a path for diagnosing plasma conditions in this material.

The gas-puff and wire-array examples presented above both employed low-percentage dopants, which limited opacity and allowed us to see Doppler-split oval line profiles. Many wire arrays do not have suitable dopants, however, and the line emission is strongly influenced by opacity. Opacity may broaden and attenuate the red- and blue-shifted components, obscuring the splitting. In the wire-array case, the Al He- α

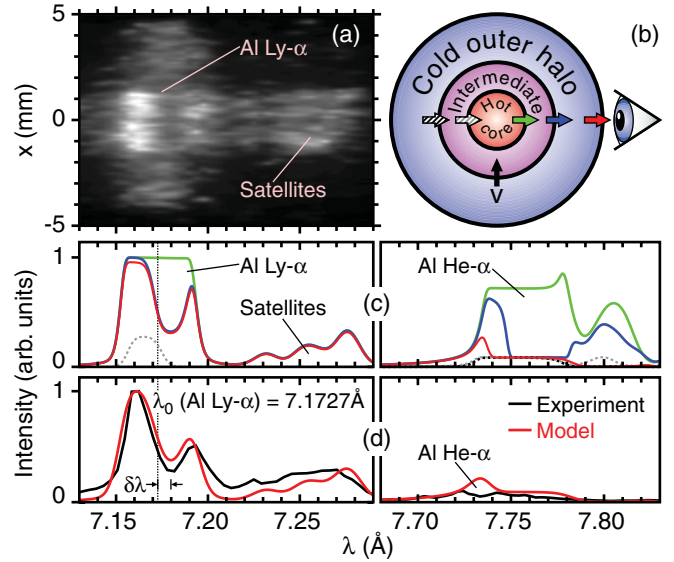


FIG. 6. (Color) (a) Imaged K -shell spectrum from a high-mass Al wire array (Z1518) shows asymmetry in the Al Ly- α line shape near $x = 0$ due to red-shifted absorption. (b) A three-shell model is considered, with the hot core backlighting the imploding outer layers. (c) The modeled spectra transported at each zone boundary indicated by a corresponding colored arrow in (b). (d) The modeled spectrum seen by the observer is smoothed according to instrumental resolution (red) and compared to an $x = 0$ lineout through (a).

and Ly- α lines show no Doppler splitting at the same times when the Mg He- α ovals are apparent. In addition, a more massive 5.9-mg/cm, 20-mm-diameter Al wire array exhibited no Mg dopant Doppler splitting. The implosion velocity can still be inferred from Doppler-shifted absorption, however. Figure 6(a) shows a spatially resolved spectrum in the vicinity of the Al Ly- α line recorded at the foot of the x-ray pulse (-13 ns relative to peak power for this heavier load). Bright emission from this resonance line and its satellites is seen from a Z -pinch core 3 mm in diameter. The line shape is asymmetric, which we show is due to a red-shifted absorption line produced by trailing mass backlit by emission from the core.

To address Doppler-shifted absorption quantitatively, we consider the three-coaxial-shell model in Fig. 6(b). Our strategy in this analysis is to generate a model including a brightly emitting core surrounded by cooler outer layers, which can have significant opacity in the x-ray lines of interest. The plasma conditions in each layer produce emission and absorption per numerical atomic kinetics and are coupled with self-consistent radiative transfer calculations to generate a synthetic spectrum. We iterate on specifying the plasma parameters in each zone in order to produce a radiated spectrum that agrees well with the experiment.

In this model, the radius of the core is 1.5 mm based on the size of the bright on-axis region of Al line emission, the intermediate region boundary is taken as 4.5 mm as dim Al Ly- α emission is seen to at least that radius (limited by spectrometer field of view), and the halo size is taken as the initial wire-array radius. These distinct shells approximate spatial gradients in the plasma, and as we will discuss we

are forced to take a minimum of three zones in order to match the spectral features of interest. Ion density, electron temperature, and plasma implosion velocity are chosen in each cylindrical shell so that the emerging spectrum calculated with a time-dependent collisional-radiative kinetic model [46] matches Al Ly- α , He- α , and satellite features and the radiated K -shell power in a sequence of frames. Stark broadening is small in our case, and line shapes (and opacities) are determined by the ion motion, represented in each shell by a Gaussian velocity distribution and a radial implosion velocity obtained from the fit. The curves in Fig. 6(c) represent the modeled spectrum resulting from solving the equation of radiative transfer through a series of zones to the boundary indicated by the like-colored arrow in Fig. 6(b). We step across the $\sim 4 \times 10^{19} \text{ cm}^{-3}$ plasma toward the observer in this way and consider the role of the various zones in determining the final spectral shape.

We begin on the far side of the plasma from the observer and consider the spectrum emitted from the halo region and passing into the intermediate layer [hatched black arrow in Fig. 6(b)]. The halo plasma on the far side away from the observer contributes only a very small amount to Al He- α [dashed black curve in Fig. 6(c)]. Next, we look at the modeled spectrum emitted from the intermediate layer toward the core (hatched gray arrow). This far side of the intermediate zone contributes only a little to Al Ly- α (dashed gray curve). Stepping across the ~ 350 -eV core, we then consider the spectrum emerging from the core plasma at the location of the green arrow. From the green curve in Fig. 6(c), we see bright emission of Al Ly- α and satellites, as well as Al He- α . These lines are flattened at their peaks by opacity in the core and serve to backlight the remaining plasma between the core and observer. The spectrum of radiation passing out of the intermediate layer toward the observer (blue arrow) is shown in Fig. 6(c) (blue curve). The ~ 250 -eV intermediate layer is hot enough to maintain a ground-state H-like Al population, which generates an Al Ly- α absorption line, red-shifted because this plasma layer is imploding at $16 \pm 3 \text{ cm}/\mu\text{s}$. The larger relative error here is due to uncertainty in identifying line center λ_0 in establishing the dispersion axis for the data; this is not a contributing factor when measuring a red or blue Doppler split. We then simulate the final spectrum that is radiated along a chord through the Z -pinch axis toward the observer [red arrow in Fig. 6(b) and red curve in Fig. 6(c)]. The third ~ 50 -eV halo zone, with no H-like ions but with some He-like ions mostly in the ground state, is required to attenuate the Al He- α line to the level seen in the experiment while not perturbing the Al Ly- α line shape.

Figure 6(d) shows a lineout ($x = 0$, $\Delta x = 3 \text{ mm}$) across the core in Fig. 6(a) (black), and the final modeled spectrum (red) emerging from the plasma is shown here convolved with the instrumental resolution. The agreement is quite reasonable and includes an asymmetric Al Ly- α line shape due to the interplay of Doppler shifts, spatial gradients, and opacity. While this zoned treatment of gradients in the plasma is approximate, it does explain the observed line structure and is consistent with plasma inflow producing red-shifted absorption from which a Doppler velocity can be inferred. This phenomenon is seen in P Cygni profiles of massive stars where outgoing winds in the stellar atmosphere create blue-shifted absorption lines

superimposed on the unshifted emission from the star's core [47,48].

IV. SUMMARY AND DISCUSSION

We have shown that low-opacity dopants can be used to measure velocity at the beginning of the stagnation phase of fast Z pinches via Doppler splitting of x-ray lines. The technique is demonstrated on the Z machine for both gas-puff and wire-array loads. These data are valuable for understanding energy balance; they provide information on kinetic energy coupling and will help to validate numerical stagnation models. The 3D MHD modeling of a wire-array implosion presented here suggests that a reasonable approach to constraining the model is to construct synthetic diagnostic data and compare the emissivity-weighted Doppler velocities between the model and the experiment. Initial comparisons of this sort using a tabulated total x-ray emissivity to construct synthetic line profiles produced a remarkable $\sim 15\%$ agreement between modeled and measured velocities. Using a tabulated emissivity model calculated for the specific line for which Doppler splitting is observed may allow a better comparison. According to the 3D MHD simulation, when integrated over both the implosion and stagnation, the $(\mathbf{j} \times \mathbf{B})$ -coupled energy is sufficient to explain the radiated energy without resorting to anomalous heating mechanisms. This is an important conclusion that continues to be explored in a variety of Z -pinch loads on Z . Employing Doppler spectroscopy is expected to provide a useful constraint on the plasma velocities, which may help to build confidence in the kinetic energy coupling calculated by implosion codes.

With only high-opacity lines available, Doppler-shifted absorption features may be used to infer velocity. In this case, emission from a hot core backlights the cooler imploding mass surrounding the core, and the Doppler shift of the resulting absorption feature provides information on the velocity of the trailing material. This phenomenon has been observed in an Al wire-array experiment and, while the analysis is challenging, it does not rely on introducing a dopant to the experiment in order to infer velocity. The multizone model presented, including atomic physics and radiative transfer calculations, provides additional information on plasma conditions and gradients. A tabular approach to 3D transport and modeling of Doppler-shifted lines from non-LTE plasmas is also being developed [49].

Other techniques may be employed to measure bulk velocity, and each has advantages and disadvantages compared to the measurements presented here. Radially resolved optical streak camera data [50] provide a continuous trajectory measurement with ± 10 – 15% errors in inferred velocity [51]. Gated extreme ultraviolet (XUV) pinhole cameras [52] provide unique 2D imaging data with approximately $\pm 10\%$ errors in velocity [51] associated with fitting a multipoint trajectory. In both of these cases, the apparent velocity of the emitting plasma is measured, although comparison of XUV imaging with laser probing suggests that the emission front corresponds to a mass snowplow front in low-current Z pinches [51]. Prior comparison of x-ray pinhole camera and radial optical streak data from tungsten wire arrays on the Z machine provided velocities corresponding to the inner edge of the implosion that were 40% faster than velocities at the outer edge [38].

This suggests that there can be significant velocity gradients in the imploding material and that a different apparent velocity can be measured depending on the range of spectral response of the diagnostic. Doppler spectroscopy measures actual particle velocity using each frame of data, with accuracy of less than $\pm 5\%$ possible as presented here. Doppler techniques have a distinct advantage over velocity inferences from self-emission trajectory measurements, which could actually show the phase velocity of an ionization wave or emitting shock front. All of these techniques provide velocity information regarding only the region of plasma that is emitting the radiation of interest, and care must be taken in the interpretation of the measured velocity. An emissivity-weighted average velocity may differ from the center-of-mass velocity and thus does not necessarily indicate the net plasma kinetic energy associated with radial motion. For this reason, we have pursued comparison of the measured data directly to synthetic diagnostic data as a method for making a clear comparison.

Multiframe radiography on Z may allow inference of the plasma velocity and kinetic energy, imaging the full extent of the mass profile rather than being limited to the region emitting a particular line of interest. However, in the present Z backlighter configuration, a rod on axis is required to quench time-integrated self-emission that would otherwise contaminate the radiograph [24]. The development of a gated detector or a higher energy backlighter may eliminate this contamination. Doppler spectroscopy of x-ray line self-emission presently allows study of pinch stagnation on a bare axis, with measurement of plasma velocity at the final stage of implosion very close to the axis. Future observation of lines emitted from the cooler trailing material may allow study of velocities in a greater fraction of the plasma.

Thomson scattering diagnostics can show Doppler shifts of spectral features and thus yield bulk velocities and like K -shell line ratio analyses can also provide information on plasma temperature and density. Demonstrated in laser-produced plasmas [53] at similar electron temperatures and densities to those obtained in cylindrical implosions on Z , these techniques are presently in development for application to dense Z pinches [54]. It may prove difficult to measure plasma conditions near pinch stagnation, where a weak scattered

signal may be overwhelmed by intense emission from the Z pinch. Interpretation of the scattered spectrum may also be complicated by the nonuniform 3D structure present in wire array implosions; however, Thomson scattering is a powerful diagnostic technique that is certainly worth pursuing.

In presenting the Doppler spectroscopy techniques applied to pinches on the Z machine, we have emphasized key features of the instrumentation that allow these phenomena to be observed quantitatively. Time resolution is critical for observing Doppler features in the imploding shell, minimizing motional blurring so that velocity changes can be measured. With no time gating, Doppler splitting and shifted absorption features would be obscured by the extremely intense emission that occurs when the plasma stagnates on axis. Spatial resolution is also crucial in order to resolve the Doppler features along a chordal view passing through the axis of the Z pinch ($x = 0$). It also provides additional information on the radial region at which the specific line emission is generated. One could forego observation of the radial structure and instead employ a slit aperture parallel to the z axis positioned near the source and aligned with the viewing chord passing through $x = 0$. This would allow accurate measurement of Doppler shifts with a view parallel to the radial velocity [i.e., line shapes per Fig. 1(g)] and could accommodate a streak camera detector for higher time resolution of the spectral measurements.

Time- and space-resolved Doppler spectroscopy may be useful for other laboratory plasmas such as imploding capsules or high-energy-density experiments studying bulk flows.

ACKNOWLEDGMENTS

The authors thank the Z operations and diagnostic teams for supporting these experiments and J. L. Giuliani (Naval Research Laboratory) and B. Balick (University of Washington) for valuable discussions. Sandia National Laboratories is a multiprogram laboratory managed and operated by Sandia Corporation, a wholly owned subsidiary of Lockheed Martin Corporation, for the US Department of Energy's National Nuclear Security Administration under Contract No. DE-AC04-94AL85000.

-
- [1] H. M. Antia, *Curr. Sci. India* **97**, 911 (2009).
 - [2] R. W. Walsh and J. Ireland, *Astron. Astrophys. Rev.* **12**, 1 (2003).
 - [3] M. Mayor and D. Queloz, *Nature (London)* **378**, 355 (1995).
 - [4] G. Marcy and P. Butler, *Astrophys. J.* **464**, L153 (1996).
 - [5] J. M. Comerford, B. F. Gerke, J. A. Newman, M. Davis, R. Yan, M. C. Cooper, S. M. Faber, D. C. Koo, A. L. Coil, D. J. Rosario, and A. A. Dutton, *Astrophys. J.* **698**, 956 (2009).
 - [6] M. Bitter, K. W. Hill, M. Zarnstorff, S. von Goeler, R. Hulse, L. C. Johnson, N. R. Sauthoff, S. Sesnic, K. M. Young, M. Tavernier, F. Bely-Dubau, P. Faucher, M. Cornille, and J. Dubau, *Phys. Rev. A* **32**, 3011 (1985).
 - [7] B. C. Stratton, M. Bitter, K. W. Hill, D. L. Hillis, and J. T. Hogan, *Fusion Sci. Technol.* **53**, 431 (2008).
 - [8] M. R. Brown, C. D. Cothran, and J. Fung, *Phys. Plasmas* **13**, 056503 (2006).
 - [9] J. D. Perez, L. F. Chase, R. E. McDonald, L. Tannenwald, and B. A. Watson, *J. Appl. Phys.* **52**, 670 (1981).
 - [10] R. E. Stewart, D. D. Dietrich, P. O. Egan, R. J. Fortner, and R. J. Dukart, *J. Appl. Phys.* **61**, 126 (1987).
 - [11] T. Nash, C. Deeney, P. D. LePell, R. Prasad, and M. Krishnan, *Rev. Sci. Instrum.* **61**, 2810 (1990).
 - [12] M. E. Foord, Y. Maron, G. Davara, L. Gregorian, and A. Fisher, *Phys. Rev. Lett.* **72**, 3827 (1994).
 - [13] R. B. Spielman, C. Deeney, G. A. Chandler, M. R. Douglas, D. L. Fehl, M. K. Matzen, D. H. McDaniel, T. J. Nash, J. L. Porter, T. W. L. Sanford, J. F. Seamen, W. A. Stygar, K. W. Struve, S. P. Breeze, J. S. McGurn, J. A. Torres, D. M. Zagor,

- T. L. Gilliland, D. O. Jobe, J. L. McKenney, R. C. Mock, M. Vargas, T. Wagoner, and D. L. Peterson, *Phys. Plasmas* **5**, 2105 (1998).
- [14] M. K. Matzen, M. A. Sweeney, R. G. Adams, J. R. Asay, J. E. Bailey, G. R. Bennett, D. E. Bliss, D. D. Bloomquist, T. A. Brunner, R. B. Campbell, G. A. Chandler, C. A. Coverdale, M. E. Cuneo, J.-P. Davis, C. Deeney, M. P. Desjarlais, G. L. Donovan, C. J. Garasi, T. A. Haill, C. A. Hall, D. L. Hanson, M. J. Hurst, B. Jones, M. D. Knudson, R. J. Leeper, R. W. Lemke, M. G. Mazarakis, D. H. McDaniel, T. A. Mehlhorn, T. J. Nash, C. L. Olson, J. L. Porter, P. K. Rambo, S. E. Rosenthal, G. A. Rochau, L. E. Ruggles, C. L. Ruiz, T. W. L. Sanford, J. F. Seamen, D. B. Sinars, S. A. Slutz, I. C. Smith, K. W. Struve, W. A. Stygar, R. A. Vesey, E. A. Weinbrecht, D. F. Wenger, and E. P. Yu, *Phys. Plasmas* **12**, 055503 (2005).
- [15] L. Gregorian, E. Kroupp, G. Davara, A. Starobinets, V. I. Fisher, V. A. Bernshtam, Yu. V. Ralchenko, Y. Maron, A. Fisher, and D. H. H. Hoffmann, *Phys. Rev. E* **71**, 056402 (2005).
- [16] L. Gregorian, E. Kroupp, G. Davara, V. I. Fisher, A. Starobinets, V. A. Bernshtam, A. Fisher, and Y. Maron, *Phys. Plasmas* **12**, 092704 (2005).
- [17] L. Gregorian, V. A. Bernshtam, E. Kroupp, G. Davara, and Y. Maron, *Phys. Rev. E* **67**, 016404 (2003).
- [18] E. Kroupp, D. Osin, A. Starobinets, V. Fisher, V. Bernshtam, Y. Maron, I. Uschmann, E. Förster, A. Fisher, and C. Deeney, *Phys. Rev. Lett.* **98**, 115001 (2007).
- [19] C. A. Jennings, M. E. Cuneo, E. M. Waisman, D. B. Sinars, D. J. Ampleford, G. R. Bennett, W. A. Stygar, and J. P. Chittenden, *Phys. Plasmas* **17**, 092703 (2010).
- [20] L. I. Rudakov, A. L. Velikovich, J. Davis, J. W. Thornhill, J. L. Giuliani Jr., and C. Deeney, *Phys. Rev. Lett.* **84**, 3326 (2000).
- [21] A. Yu. Labetsky, R. B. Baksht, V. I. Oreshkin, A. G. Rousskikh, and A. V. Shishlov, *IEEE T. Plasma Sci.* **30**, 524 (2002).
- [22] K. G. Whitney, J. W. Thornhill, J. P. Apruzese, J. Davis, C. Deeney, and C. A. Coverdale, *Phys. Plasmas* **11**, 3700 (2004).
- [23] M. G. Haines, P. D. LePell, C. A. Coverdale, B. Jones, C. Deeney, and J. P. Apruzese, *Phys. Rev. Lett.* **96**, 075003 (2006).
- [24] D. B. Sinars, R. W. Lemke, M. E. Cuneo, S. V. Lebedev, E. M. Waisman, W. A. Stygar, B. Jones, M. C. Jones, E. P. Yu, J. L. Porter, and D. F. Wenger, *Phys. Rev. Lett.* **100**, 145002 (2008).
- [25] C. Deeney, M. R. Douglas, R. B. Spielman, T. J. Nash, D. L. Peterson, P. L'Eplattenier, G. A. Chandler, J. F. Seamen, and K. W. Struve, *Phys. Rev. Lett.* **81**, 4883 (1998).
- [26] C. A. Coverdale, B. Jones, D. J. Ampleford, J. Chittenden, C. Jennings, J. W. Thornhill, J. P. Apruzese, R. W. Clark, K. G. Whitney, A. Dasgupta, J. Davis, J. Giuliani, P. D. LePell, C. Deeney, D. B. Sinars, and M. E. Cuneo, *High Energy Dens. Phys.* **6**, 143 (2010).
- [27] W. W. Campbell and J. H. Moore, *Pub. Lick Obs.* **13**, 75 (1918).
- [28] A. R. Hajian, S. M. Movit, D. Trofimov, B. Balick, Y. Terzian, K. H. Knuth, D. Granquist-Fraser, K. A. Huysen, A. Jalobeanu, D. McIntosh, A. E. Jaskot, S. Palen, and N. Panagia, *Astrophys. J. Suppl. S.* **169**, 289 (2007).
- [29] J. E. Bailey, G. A. Chandler, S. A. Slutz, I. Golovkin, P. W. Lake, J. J. MacFarlane, R. C. Mancini, T. J. Burris-Mog, G. Cooper, R. J. Leeper, T. A. Mehlhorn, T. C. Moore, T. J. Nash, D. S. Nielsen, C. L. Ruiz, D. G. Schroen, and W. A. Varnum, *Phys. Rev. Lett.* **92**, 085002 (2004).
- [30] P. W. Lake, J. E. Bailey, G. A. Rochau, T. C. Moore, D. Petmecky, and P. Gard, *Rev. Sci. Instrum.* **75**, 3690 (2004).
- [31] C. A. Coverdale, C. Deeney, A. L. Velikovich, J. Davis, R. W. Clark, Y. K. Chong, J. Chittenden, S. Chantrenne, C. L. Ruiz, G. W. Cooper, A. J. Nelson, J. Franklin, P. D. LePell, J. P. Apruzese, J. Levine, and J. Banister, *Phys. Plasmas* **14**, 056309 (2007).
- [32] C. A. Coverdale, C. Deeney, A. L. Velikovich, R. W. Clark, Y. K. Chong, J. Davis, J. Chittenden, C. L. Ruiz, G. W. Cooper, A. J. Nelson, J. Franklin, P. D. LePell, J. P. Apruzese, J. Levine, J. Banister, and N. Qi, *Phys. Plasmas* **14**, 022706 (2007).
- [33] E. M. Waisman, M. E. Cuneo, W. A. Stygar, R. W. Lemke, K. W. Struve, and T. C. Wagoner, *Phys. Plasmas* **11**, 2009 (2004).
- [34] J. P. Apruzese, K. G. Whitney, J. Davis, and P. C. Kepple, *J. Quant. Spectrosc. Radiat. Transfer* **57**, 41 (1997).
- [35] S. H. Glenzer, C. A. Back, K. G. Estabrook, B. J. MacGowan, D. S. Montgomery, R. K. Kirkwood, J. D. Moody, D. H. Munro, and G. F. Stone, *Phys. Rev. E* **55**, 927 (1997).
- [36] S. B. Hansen, J. Bauche, C. Bauche-Arnoult, and M. F. Gu, *High Energy Dens. Phys.* **3**, 109 (2007).
- [37] H. A. Scott and S. B. Hansen, *High Energy Dens. Phys.* **6**, 39 (2010).
- [38] M. E. Cuneo, D. B. Sinars, E. M. Waisman, D. E. Bliss, W. A. Stygar, R. A. Vesey, R. W. Lemke, I. C. Smith, P. K. Rambo, J. L. Porter, G. A. Chandler, T. J. Nash, M. G. Mazarakis, R. G. Adams, E. P. Yu, K. W. Struve, T. A. Mehlhorn, S. V. Lebedev, J. P. Chittenden, and C. A. Jennings, *Phys. Plasmas* **13**, 056318 (2006).
- [39] D. B. Sinars, M. E. Cuneo, E. P. Yu, D. E. Bliss, T. J. Nash, J. L. Porter, C. Deeney, M. G. Mazarakis, G. S. Sarkisov, and D. F. Wenger, *Phys. Rev. Lett.* **93**, 145002 (2004).
- [40] D. B. Sinars, M. E. Cuneo, B. Jones, C. A. Coverdale, T. J. Nash, M. G. Mazarakis, J. L. Porter, C. Deeney, D. F. Wenger, R. G. Adams, E. P. Yu, D. E. Bliss, and G. S. Sarkisov, *Phys. Plasmas* **12**, 056303 (2005).
- [41] D. L. Peterson, R. L. Bowers, K. D. McLenithan, C. Deeney, G. A. Chandler, R. B. Spielman, M. K. Matzen, and N. F. Roderick, *Phys. Plasmas* **5**, 3302 (1998).
- [42] J. P. Chittenden, S. V. Lebedev, C. A. Jennings, S. N. Bland, and A. Ciardi, *Plasma Phys. Control. Fusion* **46**, B457 (2004).
- [43] S. V. Lebedev, F. N. Beg, S. N. Bland, J. P. Chittenden, A. E. Dangor, and M. G. Haines, *Phys. Plasmas* **9**, 2293 (2002).
- [44] S. V. Lebedev, J. P. Chittenden, S. N. Bland, D. J. Ampleford, C. Jennings, and M. G. Haines, *AIP Conf. Proc.* **651**, 65 (2002).
- [45] E. P. Yu, M. E. Cuneo, M. P. Desjarlais, R. W. Lemke, D. B. Sinars, T. A. Haill, E. M. Waisman, G. R. Bennett, C. A. Jennings, T. A. Mehlhorn, T. A. Brunner, H. L. Hanshaw, J. L. Porter, W. A. Stygar, and L. I. Rudakov, *Phys. Plasmas* **15**, 056301 (2008).
- [46] V. I. Fisher, D. V. Fisher, and Y. Maron, *High Energy Dens. Phys.* **3**, 283 (2007).
- [47] M. Maury, *Ann. Harvard Coll. Obs.* **28**, 101 (1897).
- [48] G. Israelian and M. D. Groot, *Space Sci. Rev.* **90**, 493 (1999).
- [49] S. B. Hansen, B. Jones, J. L. Giuliani, J. P. Apruzese, J. W. Thornhill, H. A. Scott, D. J. Ampleford, C. A. Jennings, C. A. Coverdale, M. E. Cuneo, G. A. Rochau, J. E. Bailey,

- A. Dasgupta, R. W. Clark, and J. Davis, [High Energy Dens. Phys. 7, 303 \(2011\)](#).
- [50] S. V. Lebedev, F. N. Beg, S. N. Bland, J. P. Chittenden, A. E. Dangor, M. G. Haines, S. A. Pikuz, and T. A. Shelkovenko, [Laser Part. Beams 19, 355 \(2001\)](#).
- [51] S. N. Bland and S. V. Lebedev (private communication).
- [52] S. N. Bland, S. V. Lebedev, J. P. Chittenden, G. N. Hall, F. Suzuki-Vidal, D. J. Ampleford, S. C. Bott, J. B. A. Palmer, S. A. Pikuz, and T. A. Shelkovenko, [Phys. Plasmas 14, 056315 \(2007\)](#).
- [53] S. H. Glenzer, W. E. Alley, K. G. Estabrook, J. S. De Groot, M. G. Haines, J. H. Hammer, J.-P. Jadaud, B. J. MacGowan, J. D. Moody, W. Rozmus, L. J. Suter, T. L. Weiland, and E. A. Williams, [Phys. Plasmas 6, 2117 \(1999\)](#).
- [54] A. Harvey-Thompson, S. V. Lebedev, S. Patankar, R. Smith, H. W. Doyle, S. N. Bland, J. P. Chittenden, G. N. Hall, F. Suzuki Vidal, G. Swadling, G. Burdiak, P. D. Grouchy, L. Pickworth, E. Khoory, L. Suttle, and A. Colaitis, Proceedings of the 38th IEEE Int. Conf. Plasma Sci. (unpublished).